Nuclear-Magnetic-Resonance-Imaging-Based Capillary Rheometer

Man Ken Cheung
Dept. of Applied Biology and Chemical Technology, Hong Kong Polytechnic University, Kowloon, Hong Kong

Robert L. Powell
Dept. of Chemical Engineering and Materials Science, University of California, Davis, CA 95616

Michael J. McCarthy
Dept. of Food Science and Technology, University of California, Davis, CA 95616

This is a followup to Powell et al.'s (1994) suggestion of using nuclear magnetic resonance imaging (NMRI) for viscosity measurements. Three models are examined for non-Newtonian fluid: power law, Bingham plastic, and Herschel-Bulkley. It also demonstrates that rheological properties based on these models may be extracted from a single NMRI-measured velocity profile. Either a time-of-flight (McCarthy et al., 1991) or a phase encoding method (Seymour et al., 1993; Li et al., 1994, 1995) can be used to measure the velocity profile. The range of shear rates measured can be varied by changing the flow rate or pressure drop. This NMRI-based viscometric technique can be applied to opaque as well as transparent fluids and, hence, has the potential for industrial applications ranging from thermoplastics to highly dense suspensions (Manavel et al., 1996).

This technique involves directly using images of steady-state laminar flow profiles, and an auxiliary measurement of the pressure drop ΔP. The theory rests on two simple observations. First, independent of the constitutive relation for the material, conservation of linear momentum prescribes that the shear stress σ as a function of the radial position in the tube r through

$$\sigma(r) = r\frac{\Delta P}{2L} \tag{1}$$

where $\Delta P/L$ is the pressure gradient. Second, the shear rate is simply calculated from the measured velocity profile using

$$\dot{\gamma}(r) = -\frac{dv}{dr} \tag{2}$$

where v is the axial velocity. By eliminating r in Eqs. 1 and 2, the shear stress vs. shear rate can be obtained. Formally, if we invert Eq. 2 to obtain $r(\dot{\gamma})$ and then substitute into Eq. 1, we find $\sigma(\dot{\gamma})$, or $\eta(\dot{\gamma}) = \sigma\dot{\gamma}/\dot{\gamma}$. More importantly, these equations show that from a single velocity profile imaged at a specific value of $\Delta P/L$, data are obtained over shear rates theoretically ranging from zero at the tube center to the maximum shear rate at the tube wall $r = R$.

Constitutive Models

The simplest expression for non-Newtonian behavior is the power law model (Bird et al., 1960)

$$\sigma = m\dot{\gamma}^n \tag{3}$$

where m is called the consistency index, and n is the flow behavior index. For $n = 1$, it reduces to the Newtonian model with m as the fluid viscosity.

In materials such as foodstuffs, slurries and concentrated suspensions there is almost no flow, zero shear rate, until σ reaches a yield value. Toothpaste and nuclear fuel slurries are examples of Bingham plastic

$$\sigma - \sigma_o = \mu_o\dot{\gamma} \tag{4}$$

where σ_o is the dynamic or apparent yield stress, and μ_o is the plastic viscosity.

The Herschel-Bulkley model is more general than the previous two models

$$\sigma - \sigma_o = K\dot{\gamma}^{n_1} \tag{5}$$

where σ_o is the dynamic or apparent yield stress, K is the consistency index, and n_1 is the flow behavior index. Note that when $\sigma_o = 0$, Eq. 5 reduces to the power law model (Eq. 3). When $n_1 = 1$, Eq. 5 reduces to the Bingham plastic model Eq. 4.

Velocity profiles

Each of the above constitutive models has a distinct mathematical expression for the steady-state laminar flow profile. The dimensionless forms are preferred, because they can be applied in many different situations. Therefore, our data analysis procedure was written to analyze dimensionless velocity profiles.

The fully-developed laminar velocity profile of power law fluid in a circular pipe is given by (Bird et al., 1987)

$$v^* = v/v_{\max} = 1-(r^*)^{z+1} \tag{6a}$$

$$v_{\max} = \left(\frac{R\Delta P}{2Lm}\right)^z \frac{R}{z+1} \tag{6b}$$

where $z = 1/n$, and $r^* = r/R$.

The fully developed laminar velocity profile of Bingham plastic fluid is usually expressed as (Bird et al., 1960; Skelland, 1967)

$$v = \frac{R^2\Delta P}{4L\mu_o}(1-r^{*2}) - \frac{\sigma R}{\mu_o}(1-r^*); \quad r_o^* \le r^* \le 1$$

$$v = v_{\max} = \frac{R^2\Delta P}{4L\mu_o}(1-r_o^*)^2; \qquad r^* < r_o^*$$

where r_o^* is the dimensionless plug radius, r_o/R, and r_o is defined by $\sigma_o = r_o(\Delta P/2L)$. We rearrange the above expressions to the following preferred dimensionless form

$$v^* = v/v_{\max} = 1-\left(\frac{r^*-r_o^*}{1-r_o^*}\right)^2; \quad r_o^* \le r^* \le 1 \tag{7a}$$

$$v^* = v/v_{\max} = 1; \qquad r^* < r_o^*$$

$$v_{\max} = \left(\frac{R^2\Delta P}{4L\mu_o}\right)(1-r_o^*)^2 \tag{7b}$$

The steady-state laminar velocity profile for Herschel-Bulkley fluid is (Skelland, 1967)

$$v = \frac{2L}{\Delta P(z_1+1)K^{z_1}}\left[(\sigma_{\text{wall}}-\sigma_o)^{z_1+1}+(\sigma-\sigma_o)^{z_1+1}\right]; \qquad r_o^* \le r^* \le 1$$

$$v = v_{\max} = \frac{2L}{\Delta P(z_1+1)K^{z_1}}\left[(\sigma_{\text{wall}}-\sigma_o)^{z_1+1}\right]; \qquad r^* < r_o^*$$

We prefer the following dimensionless form

$$v^* = 1-\left(\frac{r^*-r_o^*}{1-r_o^*}\right)^{z_1+1}; \quad r_o^* \le r^* \le 1 \tag{8a}$$

$$v^* = 1; \qquad r^* < r_o^*$$

$$v_{\max} = \left(\frac{R\Delta P}{2LK}\right)^{z_1}\frac{R}{z_1+1}(1-r_o^*)^{z_1+1} \tag{8b}$$

where $z_1 = 1/n_1$. When $r_o^* = 0$ in Eq. 8, it reduces to Eq. 6 for the power law model. When $z_1 = 1$ in Eq. 8, it reduces to Eq. 7 for the Bingham plastic model.

Volumetric flow rates

The correct expression for the volumetric flow rate Q of the Herschel-Bulkley fluid in a circular tube should reduce to the familiar expressions for Q in the special cases of Newtonian, power law, and Bingham plastic. Assuming a no-slip condition at the tube wall, the volumetric flow rate of Herschel-Bulkley fluid becomes

$$Q = \left(\frac{R\Delta P}{2LK}\right)^{z_1}\frac{\pi R^3}{z_1+3}\left[1-\frac{z_1+3}{3}(r_o^*)^{z_1}+\frac{z_1}{3}(r_o^*)^{z_1+3}\right] \tag{9}$$

One may wish to express r_o^* as $\sigma_o/\sigma_{\text{wall}}$ instead.

For Newtonian fluid, set $z_1 = 1$, and $r_o^* = 0$ in Eq. 9, then

$$Q = \left(\frac{R\Delta P}{2LK}\right)\frac{\pi R^3}{4} = \frac{\pi R^4\Delta P}{8L\mu} \tag{10}$$

where the consistency index $K = \mu$, the viscosity. This is the well-known Hagen-Poiseuille equation.

For power law fluid, set $r_o^* = 0$ in Eq. 9, then

$$Q = \left(\frac{R\Delta P}{2Lm}\right)^z\frac{\pi R^3}{z+3} = \dot{\gamma}_{\text{wall}}\frac{\pi R^3}{z+3} \tag{11}$$

where $\dot{\gamma}_{\text{wall}}$ is the shear rate at the tube wall. This is the well-known Rabinowitsch-Mooney equation.

For Bingham plastic, set $z_1 = 1$ in Eq. 9, then

$$Q = \left(\frac{R\Delta P}{2LK}\right)\frac{\pi R^3}{4}\left[1-\frac{4}{3}(r_o^*)+\frac{1}{3}(r_o^*)^4\right] \tag{12}$$

which is the well-known Buckingham-Reiner equation.

The average velocity $\bar{v}$ can be obtained simply by dividing Q by the cross-sectional area of the pipe πR^2.

Method

Details for NMRI velocity phase encoded measurements were described previously (Powell et al., 1994; Seymour et al., 1993; Li et al., 1994a,b, 1995), and so will not be repeated here. We rather use the available space to describe the procedure to extract rheological information from the velocity profile image.

The Herschel-Bulkley model has three parameters, namely n_1, K, and r_o^*. The other two models are just a special case of the Herschel-Bulkley model. Therefore, we will describe our data analysis procedure in reference to the Herschel-Bulkley model. The derivative of Eq. 8 gives the dimensionless shear rate

$$\dot{\gamma}^* = -\frac{dv^*}{dr^*} = \left(\frac{n_1+1}{n_1}\right)\left(\frac{r^*-r_o^*}{1-r_o^*}\right)^{z_1}\left(\frac{1}{1-r_o^*}\right); \qquad r_o^* \le r^* \le 1 \tag{13}$$

Since $\sigma = r(\Delta P/2L)$ and $\sigma_o = r_o(\Delta P/2L)$, rewriting Eq. 7

$$\frac{\Delta P}{2L}(r - r_o) = K\left(\left(\frac{v_{\max}}{R}\right)\left(\frac{n_1+1}{n_1}\right)\left(\frac{r^* - r_o^*}{1-r_o^*}\right)^{z_1}\left(\frac{1}{1-r_o^*}\right)\right)^{n_1}$$

Dividing both sides by $R\Delta P/2L$ yields

$$(r^* - r_o^*) = K^*(\dot{\gamma}^*)^{n_1} \tag{14}$$

where $K^* = K(2L/R\Delta P)\ (v_{\max}/R)^{n_1}$, and $(r^* - r_o^*) = (\sigma/\sigma_{\text{wall}} - \sigma_o/\sigma_{\text{wall}})$.

For power law, simply set $r_o^* = 0$ in Eq. 14, and plot log r^* vs. log $\dot{\gamma}^*$ get n from the slope and from the intercept, $m^* = m(2L/R\Delta P)\ (v_{\max}/R)^n$ by linear regression.

For Bingham plastic, simply set $n_1 = 1$ in Eq. 14, and plot r^* vs. $\dot{\gamma}^*$ to get r_o^* from the intercept and from the slope $\mu_o^* = \mu_o(2L/R\Delta P)\ (v_{\max}/R)$ by linear regression.

Because the Herschel-Bulkley model is a 3-parameter model, some sort of iteration scheme is required:

(1) First estimate a value for r_o^* from the velocity profile data.

(2) Plot log $(r^* - r_o^*)$ vs. log $(\dot{\gamma}^*)$ to get n_1 from the slope and K^* from the intercept.

(3) Check the estimated r_o^* by plotting r^* vs. $K^*(\dot{\gamma}^*)^{n_1}$ If r_o^* was an accurate estimation, then the slope is exactly equal to 1, and the intercept is exactly equal to r_o^*.

(4) Otherwise, if slope < 1, increment the value of r_o^* for say by 5% or if slope > 1, decrement the value of r_o^* by 5%.

Repeat steps (2)–(4) until the absolute value of (slope $- 1$) ≤ 0.001.

Since we know the expressions for $v_{\max}$ from Eqs. 6b, 7b and 8b then the following relations are found

Power law:

$$m^* = m\frac{2L}{R\Delta P}\left(\frac{v_{\max}}{R}\right)^n = \left(\frac{n}{n+1}\right)^n \tag{15}$$

Bingham plastic:

$$\mu_o^* = \mu_o\frac{2L}{R\Delta P}\left(\frac{v_{\max}}{R}\right) = \frac{1}{2}(1-r_o^*)^2 \tag{16}$$

Herschel-Bulkley:

$$K^* = K\frac{2L}{R\Delta P}\left(\frac{v_{\max}}{R}\right)^{n_1} = \left(\frac{n_1}{n_1+1}\right)^{n_1}(1-r_o^*)^{1+n_1} \tag{17}$$

The above relations may be used to validate or to check how accurate a particular model in describing the non-Newtonian fluid of interest, and to check the accuracy of the measured data.

Results and Discussion

In our previous note (Powell et al., 1994), we used a simple centered differences of the velocity profile to determine the shear rate. Those shear rates displayed the right trend in the shear stress vs. shear rate diagram, but they were somewhat scattered making the extraction of rheological parameters difficult. To circumvent this problem, we now use a 15th-order polynomial to first fit the velocity profile, and then taking the derivative to calculate the shear rate. For power law fluids, a 11th-order polynomial is sufficient to fit the velocity profile accurately.

Velocity fluctuations at each radial position can be due to molecular diffusion, and artifacts from the fluid pumping apparatus (Seymour et al., 1993; Arola et al., 1997a). The accuracy of the velocity gradient (shear rate) calculations, especially at the tube center, can be severely limited by the spreading in velocity. In this study, we use the maximum intensity pixel at each radial position to mark the mean velocity at that position. Then, global curve fitting the data points with a polynomial is justifiable as it gives a smoothed mean velocity profile. We dropped the data points near the tube center (zero shear rates) from data analysis to extract rheological parameters.

At this low shear rates region, the velocity resolution and shear rates are comparable in size, and so the calculated shear viscosities will have large uncertainties (Arola et al., 1997a). Nevertheless, shear rates ranging over two decades of magnitude are used in calculating the rheological parameters. We recognize the difficulty in calculating derivatives from measured data accurately. In fact, finding the optimal method for doing such a calculation is an unsolved problem. However, the engineering approach suggested here is a popular one because polynomials are simple to handle mathematically, and is feasible for quality control and process monitoring applications.

Figure 1 shows a dimensionless velocity distribution of a 3 wt. % aqueous polyacrylamide solution. The maximum velocity is 3.625 cm/s. The present procedure yields a power law flow behavior index $n = 0.512 \pm 0.005$, and a dimensionless power law consistency index $m^* = 0.600 \pm 0.002$. The uncer-

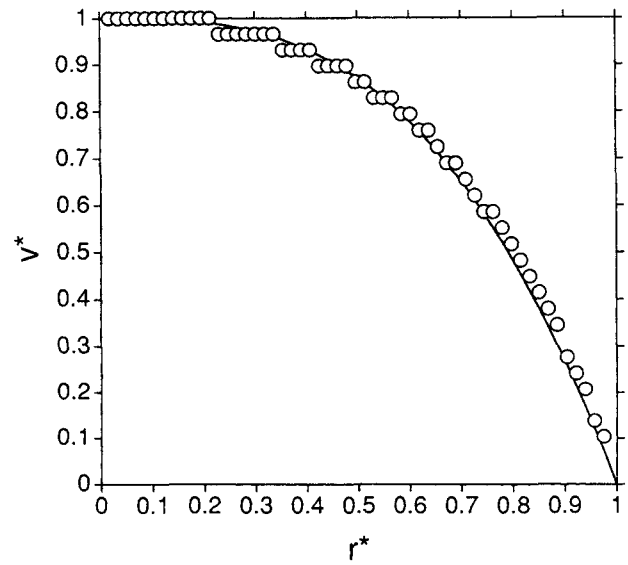

Figure 1. Velocity distribution of a 3% wt. aqueous polyacrylamide solution (circles).

The velocity is normalized by the maximum velocity 3.625 cm/s. The solid line is the power law velocity distribution with $n = 0.512 \pm 0.005$, and $m^* = 0.600 \pm 0.002$. The square of the correlation coefficient is 0.998.

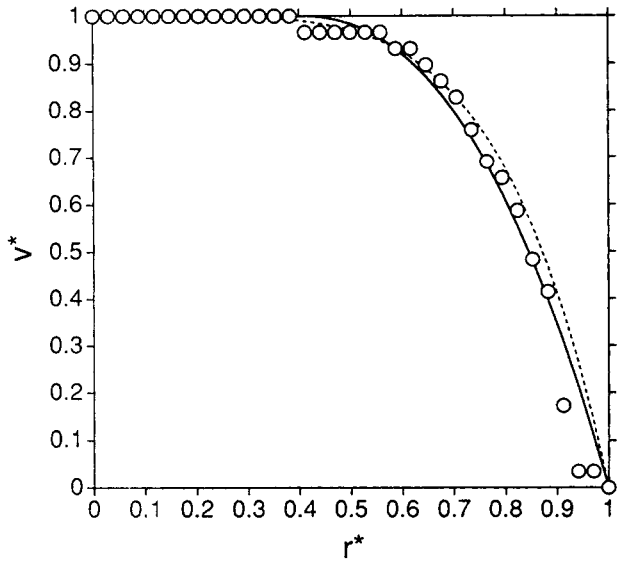

Figure 2. Velocity distribution of a 6.3% solids tomato juice (circles).

The velocity is normalized by the maximum velocity 5.438 cm/s. The solid line is the Herschel-Bulkley velocity distribution with $n_1 = 0.746 \pm 0.013$, $K^* = 0.182 \pm 0.002$, and $r_o^* = 0.396 \pm 0.003$. The broken line is the power law velocity distribution with $n = 0.247 \pm 0.005$, and $m^* = 0.628 \pm 0.002$. The square of the correlation coefficient for the Herschel-Bulkley model is 0.994, and that for the power law model is 0.991.

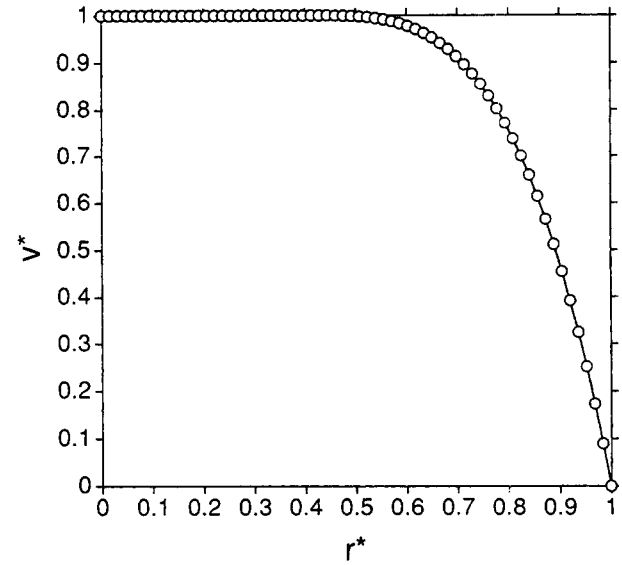

Figure 3. Herschel-Bulkley model velocity profile generated with $n_1 = 0.4$ and $r_o^* = 0.4$ (exact values) is plotted with circles.

The solid line is the profile determined by the data analysis procedure; $n_1 = 0.4052 \pm 0.0001$, $K^* = 0.2933 \pm 0.0003$, and $r_o^* = 0.4031 \pm 0.0001$. The square of the correlation coefficient is 1.000.

tainty expressed here is one standard deviation. The square of the correlation coefficient for linear regression of log r^* vs. log $\dot{\gamma}^*$ is 0.998. We calculate m^* from Eq. 15 to obtain a value of 0.5744, which differs from that calculated with linear regression by merely 4%. This validates that the power law model is appropriate for describing the non-Newtonian behavior of the aqueous polyacrylamide solution. Furthermore, the power law flow behavior index $n = 0.512$ is close to that measured with a parallel plate Weissenberg rheometer 0.52 (Powell et al., 1994).

Figure 2 shows a dimensionless velocity distribution of a 6.3% solids tomato juice. The maximum velocity is 5.438 cm/s. Both the Herschel-Bulkley and the power law model are used in the food industry to describe the flow behavior of fruit juices. The Herschel-Bulkley parameters determined from this profile are $n_1 = 0.746 \pm 0.013$, $K^* = 0.182 \pm 0.002$, and $r_o^* = 0.396 \pm 0.003$. The power law parameters are $n = 0.247 \pm 0.005$, and $m^* = 0.628 \pm 0.002$. The square of the correlation coefficient for the Herschel-Bulkley model is 0.994, and for the power law model is 0.991. The pressure drop gradient, $\Delta P/L$, was measured to be 758 Pa/m. Hence, the Herschel-Bulkley consistency index K and the apparent yield stress σ_o are calculated to be 0.325 $Pa \cdot s^{n_1}$ and 2.01 Pa, respectively. The power law consistency index m is 2.26 $Pa \cdot s^n$. These values agree with those found by Rao et al. (1981). Substituting $n_1 = 0.746$, and $r_o^* = 0.396$ into Eq. 17 gives $K^* = 0.2199$, but K^* from the analysis procedure is 0.182, which is a difference of about 17%. With $n = 0.247$, Eq. 15 gives $m^* = 0.6704$, whereas m^* from linear regression of log r^* vs. log $\dot{\gamma}^*$ is 0.628, a difference of 6%. Despite that the correlation coefficient squared is very close to one, the Herschel-Bulkley parameters calculated with the present procedure are less tolerable to errors in the velocity profile than the power law model.

To check the range of applicability of the velocity profile technique, we have performed some model calculations based on the constitutive relations, Eqs. 6, 7 and 8. We first generate a model dimensionless velocity profile by inputting the necessary values: n in Eq. 6 for power law, r_o^* in Eq. 7 for Bingham plastic, and n_1 and r_o^* in Eq. 8 for Herschel-Bulkley. We then run the data analysis procedure to extract rheological parameters from the model velocity profile. The dimensionless velocity profile in Figure 3 is generated by setting $n_1 = 0.4$ and $r_o^* = 0.4$ in Eq. 8. The solid line is the profile determined by the data analysis procedure: $n_1 = 0.4052 \pm 0.0001$, $K^* = 0.2933 \pm 0.0003$, and $r_o^* = 0.4031 \pm 0.0001$. The square of the correlation coefficient for linear regression is 1.000. Substituting the calculated results for n_1 and r_o^* into Eq. 17 gives $K^* = 0.2926$, which agrees with the value of 0.2933 calculated by the procedure.

For the power law model, this procedure gives reliable flow behavior index n from the velocity profile for $0.1 < n < 1$. For Bingham plastic, reliable calculation of the dimensionless plug radius r_o^* is obtained for $0.1 < r_o^* < 0.7$. For Herschel-Bulkley model, reliable calculation of n_1 and r_o^* are obtained for $0.3 < n_1 < 1$, and $0.3 < r_o^* < 0.6$. For $n_1 > 0.4$, reliable flow behavior index n_1 and dimensionless plug radius r_o^* values can be obtained for r_o^* as small as 0.2. By the term "reliable," we mean that the difference between the calculated rheological parameter and the input parameter is 10% or smaller.

Results from the data analysis procedure can be improved with increased resolution both along the velocity and position axes, and with increased signal-to-noise ratio. Usually the improvement in resolution and signal-to-noise ratios require longer acquisition times. This is undesirable for practical industrial applications. Therefore, our group at the University of California, Davis, examine the use of velocity profile aliasing or q-space undersampling, and rapid acquisition tech-

niques to improve the velocity resolution without prolonging the measurement time (Arola et al., 1997b). The group also examines the use of Hankel transform to obtain NMRI velocity profiles of improved precision over conventional Fourier transform. Hankel transform yields true radial coordinates, whereas Fourier transform can produce apparent spreading in velocity as the result of projecting a three-dimensional profile onto a two-dimensional Cartesian plane. However, more research is needed to improve the data analysis procedures, and to optimize the NMRI experimental parameters for on-line or in-line process monitoring applications.

Conclusions

This article has demonstrated that NMRI-based rheometer yield results that compare favorably with conventional rheometrical techniques. The advantages of a NMRI-based rheometer include its ability to image opaque systems, such as filled polymeric fluids and concentrated suspensions, and its potential in an on-line or in-line process monitoring of rheological properties of complex materials.

Acknowledgments

We thank Dr. J. D. Seymour for measuring the NMRI velocity profiles, and Dr. D. F. Arola for the helpful preprints of his work.

Literature Cited

Arola, D. F., G. A. Barrall, R. L. Powell, and M. J. McCarthy, "Nuclear Magnetic Resonance Imaging-Based Viscometry," *Frontiers in Industrial Process Tomography II*, Engineering Foundation Conf., Delft, The Netherlands (Apr. 8–12, 1997a).

Arola, D. F., G. A. Barrall, R. L. Powell, and M. J. McCarthy, "Measurement Time Reducing Methods for NMR Flow Profile Imaging: Hankel Transforms, Velocity Aliasing and Rapid Repetition Time," *J. Magn. Reson. Analysis*, submitted (1997b).

Bird, R. B., W. E. Stewart, and E. N. Lightfoot, *Transport Phenomena*, Wiley, New York (1960).

Bird, R. B., R. C. Armstrong, and O. Hássager, *Dynamics of Polymeric Liquids*, Vol. 1, Wiley, New York (1987).

Li, T.-Q., R. L. Powell, M. J. McCarthy, and K. L. McCarthy, "Velocity Measurements of Fiber Suspensions in Pipe Flow by Nuclear Magnetic Resonance Imaging," *TAPPI J.*, **77**, 145 (1994a).

Li, T.-Q., M. J. McCarthy, K. L. McCarthy, J. D. Seymour, L. Ödberg, and R. L. Powell, "Visualization of the Flow Patterns of Cellulose Fiber Suspensions by Nuclear Magnetic Resonance Imaging," *AIChE J.*, **40**, 1408 (1994b).

Li, T.-Q., and K. L. McCarthy, "Pipe Flow of Aqueous Polyacrylamide Solutions Studied by Means of Nuclear Magnetic Resonance Imaging," *J. Non-Newtonian Fluid Mech.*, **57**, 155 (1995).

Maneval, J. E., K. L. McCarthy, M. J. McCarthy, and R. L. Powell, "Nuclear Magnetic Resonance Imaging Rheometer," U.S. Patent No. 5532593 (July 2, 1996).

McCarthy, K. L., R. J. Kauten, M. J. McCarthy, and J. F. Steffe, "Flow Profiles in a Tube Rheometer using Magnetic Resonance Imaging," *J. Food Engr.*, **16**, 1 (1991).

Powell, R. L., J. E. Maneval, J. D. Seymour, K. L. McCarthy, and M. J. McCarthy, "Nuclear Magnetic Resonance Imaging for Viscosity Measurements," *J. Rheo.*, **38**, 1465 (1994).

Seymour, J. D., J. E. Maneval, R. L. Powell, K. L. McCarthy, and M. J. McCarthy, "NMRI Phase Encoded Velocity Measurements of Fibrous Suspensions," *Phys. Fluids A*, **5**, 3010 (1993).

Rao, M. A., M. C. Bourne, and H. J. Cooley, "Flow Properties of Tomato Concentrates," *J. Texture Studies*, **12**, 521 (1981).

Skelland, A. H. P., *Non-Newtonian Flow and Heat Transfer*, Wiley, New York (1967).

Manuscript received Jan. 22, 1997, and revision received June 26, 1997.